

Implementation of residual nucleus de-excitations associated with proton decays in ^{12}C based on the GENIE generator and TALYS code

Hang Hu,^{1,*} Wan-Lei Guo,^{2,†} Jun Su,^{3,‡} Wei Wang,^{1,3,§} and Cenxi Yuan^{3,¶}

¹*School of Physics, Sun Yat-Sen University, Guangzhou, 510275, China*

²*Institute of High Energy Physics, Chinese Academy of Sciences, Beijing 100049, China*

³*Sino-French Institute of Nuclear Engineering and Technology, Sun Yat-Sen University, Zhuhai, 519000, China*

(Dated: May 18, 2022)

We implement the de-excitation processes of residual nuclei associated with proton decays in ^{12}C based on the GENIE generator and TALYS code. To derive the reasonable excitation energy spectra of residual nuclei ^{11}B , ^{10}B and ^{10}Be , the default GENIE nucleon decay generator is modified in terms of the Spectral Function nuclear model. Then we use the TALYS code to estimate the de-excitation processes of residual nuclei. The TALYS calculation can partly account for the experimental data.

I. INTRODUCTION

The proton decay is a generic prediction in the Grand Unified Theories (GUTs) [1, 2], since these theories put quarks and leptons into the same multiplet of the GUT gauge group. The GUTs can naturally unify the strong, weak, and electromagnetic interactions into a single underlying force at a very high energy scale. The proton decay is a crucial test of the GUTs. Although many searches have been performed over multiple decades, no experimental evidence to date for proton decay has been found [3]. The Super-Kamiokande experiment gives the best limits to the proton lifetime for most proton decay modes. In the future, three types of detectors will continue to look for the proton decay [4]: Water Cherenkov detectors [5], liquid scintillator detectors [6, 7] and liquid Argon TPC detectors [8]. Here we focus on the large liquid scintillator detectors for future proton decay searches.

The liquid scintillator (LS) as the detection medium in the past neutrino experiments has achieved great successes [9–11]. Now the next generation large LS detectors JUNO [6, 7] and LENA [12] are constructing in China and proposed in Europe, respectively. As a calorimeter, the LS detector has some specific advantages, such as its good energy resolution and a very low energy threshold, in searching for the proton decay [6, 12–16]. The initial decayed proton may be the free proton from H, or the bound proton in ^{12}C . The low energy threshold ensures that the LS detector can identify a 2.2 MeV γ -ray from the neutron captured by a proton. It can be used to separate proton decay signals from atmospheric neutrino backgrounds. Due to the excellent energy resolution, the LS experiment can measure the visible energy of daughter particles from the proton decay very well, which depends on the initial energy and momentum of the decayed proton. For the bound proton decay, one

should consider the following nuclear effects [17], Fermi motion, binding energy, and nucleon-nucleon (NN) correlation, to describe the initial state of the decayed proton. On the other hand, the final state interaction (FSI) and de-excitation processes of the residual nucleus associated with the proton decay may also change the visible energy and simultaneously produce secondary neutrons. These secondary neutrons will reduce the ability to suppress the atmospheric neutrino background through the neutron identification. To model these nuclear effects, a proton decay Monte Carlo (MC) generator is necessary for LS experiments to search for the proton decay.

GENIE is a neutrino MC generator and widely used by many neutrino experiments [18, 19]. The recent versions of GENIE can simulate more than 60 kinds of nucleon decay modes. In this paper, we used GENIE version 3.0.2 with the G18_02a_00_000 model set [19]. In this configuration of GENIE, the Bodek-Ritchie nuclear model [20] with short-range NN correlation is used for all processes, since it is simple and applicable across a broad range of target atoms and neutrino energies. For the proton decay in ^{12}C , the initial-state proton energy is limited to be a very narrow range of $910.0\text{ MeV} \leq E_p \leq 922.4\text{ MeV}$, which does not match with the measured s -shell and p -shell binding energies from the $^{12}\text{C}(e, e'p)^{11}\text{B}$ reaction [23]. On the other hand, the residual nucleus ^{11}B in GENIE would be left in the ground state. Namely, the GENIE generator does not consider the de-excitation of the residual nucleus. In fact, the Super-Kamiokande experiment has used γ -ray emissions from the de-excitation processes of ^{15}N [21] to search for $p \rightarrow \bar{\nu}K^+$ in ^{16}O [17]. For LS experiments, the neutron emission of residual nucleus is more crucial than other particle emissions. The emitted neutrons from the s -hole state of ^{11}C have been used by the KamLAND experiment to identify the neutron invisible decay mode in ^{12}C [15, 22].

In this paper, we modify the GENIE nucleon decay generator in terms of the Spectral Function (SF) nuclear model [24] to account for the nuclear effects, and then use the TALYS code [25] to implement the de-excitation processes of the residual nucleus. The JUNO has adopted this work as a part of their simulations to give a preliminary sensitivity to $p \rightarrow \bar{\nu}K^+$ [7]. This paper is or-

* huhang3@mail2.sysu.edu.cn

† guowl@ihep.ac.cn (corresponding author)

‡ sujun3@mail.sysu.edu.cn

§ wangw223@mail.sysu.edu.cn

¶ yuancx@mail.sysu.edu.cn

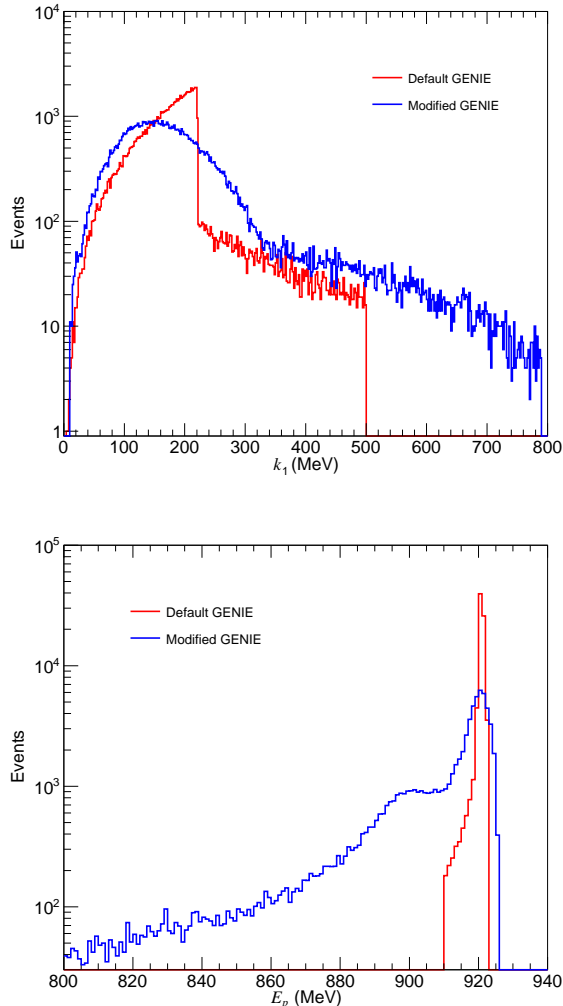


FIG. 1. Momentum (top) and energy (bottom) distributions of bound protons from ^{12}C in the default (red) and modified (blue) GENIE.

ganized as follows. In Sec. II, we present the GENIE modifications, and then show the energy and momentum distributions of bound protons in the default and modified GENIE. Sec. III describes the de-excitation processes of residual nuclei ^{11}B , ^{10}B and ^{10}Be based on the TALYS software and their excitation energy spectra. In Sec. IV, we compare the predicted results with the quasifree $^{12}\text{C}(p, 2p)^{11}\text{B}$ data. Finally, a summary will be given in Sec. V.

II. THE BOUND PROTONS IN ^{12}C

For a given proton decay mode, the energy and momentum distributions of final states only depend on those of decayed protons if we ignore the FSI and de-excitation processes of residual nucleus. The free proton from Hy-

drogen has an energy of $m_p = 938.27$ MeV and the zero momentum. Compared to the free proton, the energy and momentum of bound protons in the Carbon nucleus will be influenced by the nuclear effects [17], including the nuclear binding energy, the Fermi motion and the Nucleon-Nucleon correlations. In GENIE (version 3.0.2 with the G18_02a_00_000 model set), the Bodek-Ritchie relativistic Fermi gas nuclear model [20] with short-range NN correlation is used for all processes [18]. In this case, the off-shell energy E_p of bound protons in ^{12}C is given by

$$E_p = M_{^{12}\text{C}} - \sqrt{M_{^{11}\text{B}}^2 + k_1^2}, \quad (1)$$

where $M_{^{12}\text{C}}$ ($M_{^{11}\text{B}}$) denotes the ground-state nuclear mass of ^{12}C (^{11}B). In Fig. 1, we plot the momentum k_1 distribution of bound protons, where the tail $k_1 > 221$ MeV comes from the short-range NN correlation. By use of Eq. (1), one can easily calculate E_p as shown in the bottom panel of Fig. 1. It is found that E_p has a very narrow range of $910.0 \text{ MeV} \leq E_p \leq 922.4 \text{ MeV}$. Meanwhile, the E_p shape doesn't display the nuclear shell structure, which is not consistent with the measured s -shell and p -shell binding energies from the $^{12}\text{C}(e, e'p)^{11}\text{B}$ experiment [23]. In addition, the residual nucleus ^{11}B associated with proton decays in ^{12}C is assumed to be the ground state, which means ^{11}B does not emit any particles through the de-excitation processes.

To solve the above two problems, the off-shell energy E_p of bound protons in ^{12}C is modified by

$$E_p = M_{^{12}\text{C}} - \sqrt{M_{^{11}\text{B}^*}^2 + k_1^2}, \quad (2)$$

where $M_{^{11}\text{B}^*} = M_{^{11}\text{B}} + E_x$ and E_x is the excited energy of the residual nucleus ^{11}B . Note that Eq. (2) is usually used in the analysis of electron/neutrino scattering from a nucleon bound in a nucleus [26, 27]. Due to $k_1 \ll M_{^{11}\text{B}^*}$, we may simplify Eq. (2) and derive

$$E_p \approx m_p - (S^p + E_x + \frac{k_1^2}{2M_{^{11}\text{B}}}) = m_p - E_R, \quad (3)$$

where $S^p = M_{^{11}\text{B}} + m_p - M_{^{12}\text{C}} = 15.96$ MeV is the proton separation energy and $E_R = S^p + E_x + \frac{k_1^2}{2M_{^{11}\text{B}}}$ is defined as the removal energy [26, 27]. E_R can also be expressed by $E_R = E_B + \frac{k_1^2}{2M_{^{11}\text{B}}}$ and $E_B = S^p + E_x$ is the binding energy. In order to describe the initial state of decayed protons, we adopt the Spectral Function (SF) nuclear model [24], which provides a 2-dimensional distribution of momentum k_1 and removal energy E_R for bound protons in ^{12}C . Note that the SF model is also an optional nuclear model in GENIE. The SF nuclear model can well describe the neutrino-nucleus reactions [27–29], and could be further improved with continued experimental investigations. Based on the GENIE SF model and the modified E_p in Eq. (3), we plot the k_1 and E_p distributions in Fig. 1. It is clear that the E_p distribution shows the shell structure. The left and right peaks refer to the s -shell and p -shell protons, respectively.

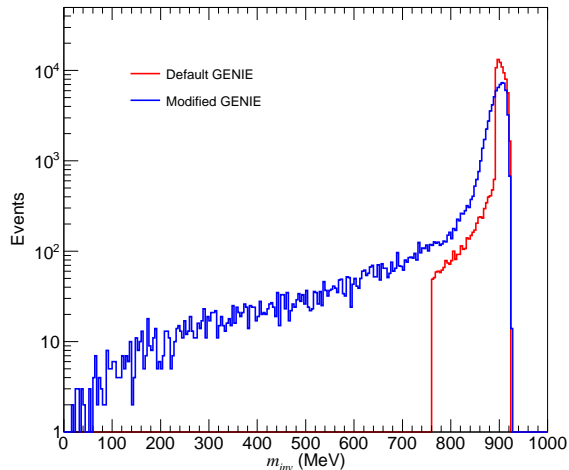


FIG. 2. Invariant mass distributions of bound protons from ^{12}C in the default (red) and modified (blue) GENIE.

With the help of k_1 and E_p , one can easily calculate the invariant mass m_{inv} of bound protons in ^{12}C . Compared with the modified GENIE, the default GENIE has a more narrow range as shown in Fig. 2. For the proton decay to be possible, the invariant mass of the initial proton has to be larger than the sum of masses of final products, namely $m_{inv} > \sum m_f$. Otherwise, this decay will be kinematically forbidden. Based on the invariant mass spectra in Fig. 2, we calculate the forbidden ratios for all possible two-body proton decay modes, including an antilepton and a meson. The forbidden ratio is defined as the fraction of the initial-state protons for which a given decay mode is kinematically forbidden. As listed in Table I, the modified GENIE has a greater forbidden ratio than the default GENIE for every proton decay mode. This is because that m_{inv} has a long tail below 760 MeV in the modified GENIE case. It is worthwhile to stress that significant differences between the default and modified GENIE can be found for some proton decay modes of $\sum m_f$ close to the proton mass.

III. DE-EXCITATION PROCESSES OF RESIDUAL NUCLEI

As mentioned above, the residual nucleus ^{11}B is always left in the ground state, and the de-excitation process is not taken into account in the default GENIE. In fact, the s -shell proton decay in ^{12}C will leave a s -hole state of ^{11}B , which de-excites by emitting n, p, d, t, α and h (^3He) particles. The previous experiments have measured some two-body de-excitation modes for the excitation energy range of $16 \text{ MeV} \leq E_x \leq 35 \text{ MeV}$ [30, 31]. For the higher E_x region or three-body de-excitation modes, we do not know the corresponding branching ratio of every de-excitation mode from the s -hole state of ^{11}B . In addition

TABLE I. Forbidden ratios of all possible two-body proton decay modes including an antilepton and a meson in the default and modified GENIE.

Decay mode	$\sum m_f$ (MeV)	Forbidden ratio (%)	
		default	modified
$p \rightarrow e^+ \pi^0$	135.5	0	0.2
$p \rightarrow \mu^+ \pi^0$	240.6	0	0.5
$p \rightarrow \bar{\nu} \pi^+$	139.6	0	0.2
$p \rightarrow e^+ \eta$	548.4	0	2.8
$p \rightarrow \mu^+ \eta$	653.5	0	4.3
$p \rightarrow e^+ \rho^0$	775.8	0.2	7.8
$p \rightarrow \mu^+ \rho^0$	880.9	5.4	28.3
$p \rightarrow \bar{\nu} \rho^+$	763.0	0	7.3
$p \rightarrow e^+ \omega$	783.2	0.4	8.2
$p \rightarrow \mu^+ \omega$	888.3	6.5	37.8
$p \rightarrow e^+ K^0$	498.1	0	2.2
$p \rightarrow \mu^+ K^0$	603.3	0	3.5
$p \rightarrow \bar{\nu} K^+$	493.7	0	2.2
$p \rightarrow e^+ K^*(892)^0$	896.1	21.5	51.2
$p \rightarrow \bar{\nu} K^*(892)^+$	891.7	7.2	43.1

tion to ^{11}B , the daughter particles of proton decays may interact with the spectator nucleons, and knock one or more of them out of ^{11}B . Due to the FSI, the residual nucleus ^{11}B may be converted to ^{10}B or ^{10}Be , and they are left in many particle-hole states. In order to determine the de-excitation processes of ^{11}B , ^{10}B and ^{10}Be , the statistical model calculation is needed. Here we shall calculate the excitation energy spectra of three kinds of residual nuclei based on the modified GENIE, and then use the TALYS code to estimate branching ratios of their de-excitation modes. TALYS is a nuclear reaction program, and is extensively used for both basic and applied science [25, 32, 33]. In Sec. IV, we shall compare the predicted branching ratios with the experimental measurements [30, 31].

A. De-excitation processes of ^{11}B states

In the modified GENIE, the excitation energy E_x can be derived from $E_x = E_R - S^p - \frac{k_1^2}{2M_{^{11}\text{B}}}$. On the other hand, one can also use the invariant mass and ground-state mass of the residual nucleus ^{11}B to calculate E_x . As shown in Fig. 3, the E_x spectrum of ^{11}B states has two peaks. The left peak (0.0 MeV) and right peak (20.2 MeV) correspond to the p -shell and s -shell proton decays in ^{12}C , respectively. Due to the NN nuclear correlation, the excitation energy E_x may be up to 300 MeV.

In a simple shell model of ^{12}C , four protons occupy the $p_{3/2}$ orbit, and two protons occupy the $s_{1/2}$ orbit. Due to pairing effects, a pair of protons may be in the $p_{1/2}$ shell in about 40% of the times [22]. In any case, 33.33% of

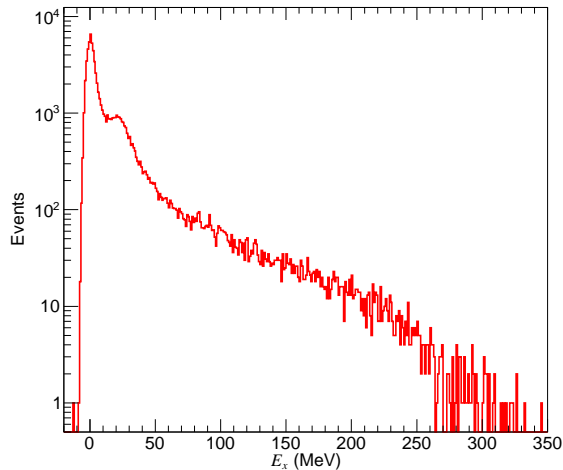


FIG. 3. Excitation energy E_x distribution of the residual nucleus ^{11}B after proton decays in ^{12}C .

^{11}B states are left in a highly excited state because of a $s_{1/2}$ proton decay. For the case of two protons in the $p_{1/2}$ shell, there is a one-third chance that the decayed protons come from the $p_{3/2}$ shell. Therefore, 13.33% of ^{11}B states are excited with medium excitation energy. For the other 53.33% possibility, the residual nucleus ^{11}B is assumed to be the ground state. Based on the E_x distribution in Fig. 3, 53.33%, 13.33%, and 33.33% possibilities correspond to $E_x \leq 6.2$ MeV, 6.2 MeV $< E_x < 15.9$ MeV, and $E_x \geq 15.9$ MeV ranges, respectively. For simplicity, we require that ^{11}B states with $E_x \leq 6.2$ MeV do not de-excite, ^{11}B states with 6.2 MeV $< E_x < 15.9$ MeV will emit a γ -ray with the energy of E_x .

For the highly excited ^{11}B states, we use the TALYS (version 1.95) code [25] to estimate the de-excitation processes via the standard “projectile 0” configuration. The inputting excitation energy grid of the initial ^{11}B population is based on the excitation energy spectrum of $E_x \geq 15.9$ MeV in Fig. 3. It has a bin width of 2 MeV and follows the spin and parity $J^\pi = 1/2^+$ format. Then the TALYS code can calculate the de-excitations of the compound nucleus ^{11}B through the multiple emission and give a summary table of exclusive cross sections. By use of the initial population cross section, one can easily obtain their branching ratios for these exclusive de-excitation modes. Note that the daughter nuclei include the contributions from both the ground state and all discrete states for every exclusive de-excitation mode. The excited daughter nucleus may decay a γ -ray into its ground state, or emit a massive particle into another nucleus. However the particle emission ratios are still unknown for some discrete states of daughter nuclei from the NNDC database [34], such as the 6th discrete level of ^{10}Be and ^9Be . So we set the number of included discrete energy levels to be 5 for ^{10}B , ^9B , ^{10}Be , ^9Be , ^8Be , ^7Be , be 3 for ^8B , ^9Li , ^8Li , ^7Li , ^6Li , and be 1 for other daughter

TABLE II. The de-excitation modes, corresponding thresholds and branching ratios from the residual nucleus ^{11}B in the case of a $s_{1/2}$ proton decay.

De-excitation Mode	Threshold (MeV)	Branching ratio (%)
$n + ^{10}\text{B}$	11.5	8.8
$p + ^{10}\text{Be}$	11.2	3.1
$d + ^9\text{Be}$	15.8	3.9
$t + ^8\text{Be}$	11.2	2.4
$\alpha + ^7\text{Li}$	8.7	2.0
$2n + ^9\text{B}$	19.9	3.5
$n + p + ^9\text{Be}$	18.0	8.9
$n + d + ^8\text{Be}$	17.5	9.8
$n + \alpha + ^6\text{Li}$	15.9	11.3
$d + \alpha + ^5\text{He}$	18.1	1.1
$t + 2\alpha$	11.2	0.9
$2n + p + ^8\text{Be}$	19.7	7.0
$n + 2p + ^8\text{Li}$	34.9	0.6
$2n + d + ^7\text{Be}$	36.4	0.5
$n + p + d + ^7\text{Li}$	34.7	1.3
$n + p + t + ^6\text{Li}$	35.7	0.7
$2n + \alpha + ^5\text{Li}$	19.9	0.9
$n + p + \alpha + ^5\text{He}$	20.3	1.9
$2n + 2p + ^7\text{Li}$	37.0	0.7
$2n + p + d + ^6\text{Li}$	42.0	0.6
other modes	-	30.2

TABLE III. The percentage of the ground state and discrete states for every daughter nucleus in Table II from the de-excitation of ^{11}B states. The definition of ratio R_A can be found in the text.

Nucleus	g.s	1st	2nd	3rd	4th	5th	R_A
^{10}B	13.2	36.2	14.1	25.9	6.3	4.3	0.141
^9B	36.7	18.9	11.4	12.1	12.7	8.1	0.263
^{10}Be	42.3	16.0	6.9	7.4	20.1	7.4	0.183
^9Be	39.3	21.7	11.0	9.9	8.3	9.8	0.303
^8Be	54.4	38.2	2.2	1.8	1.7	1.8	0.893
^7Be	37.9	34.4	9.1	8.1	7.3	3.2	0.175
^8Li	33.5	33.3	13.6	19.6	-	-	0.069
^7Li	41.6	34.5	14.4	9.6	-	-	0.216
^6Li	71.6	11.8	5.9	8.2	-	-	0.902

nuclei in the following TALYS calculations.

The predicted de-excitation modes, corresponding thresholds, and branching ratios of the highly excited ^{11}B states are listed in Table II. The percentage of the ground state and discrete states for every daughter nucleus in Table II can be found in Table III, those are calculated from their final populations after de-excitations of the continuous excited states of the corresponding nucleus. R_A in the last column of Table III describes the ratio that

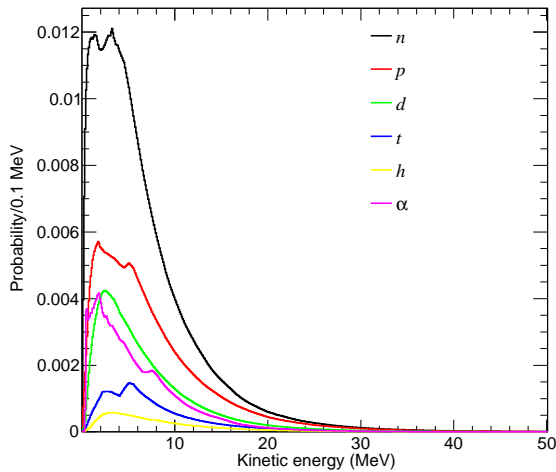


FIG. 4. The kinetic energy distributions of six kinds of outgoing particles from the de-excitation processes of highly excited ^{11}B states.

this nucleus will end up in the ground state and discrete states from its initial population after de-excitations of the continuous excited states in TALYS. Namely, the final population of the ground state and discrete states is R_A of the initial population. The other population ($1-R_A$) is converted into the lighter daughter nuclei because of the emissions of massive particles from the continuous states. From Table II, one can find that the dominant de-excitation modes, including $n+^{10}\text{B}$, $n+p+^9\text{Be}$, $n+d+^8\text{Be}$, $n+\alpha+^6\text{Li}$, $2n+p+^8\text{Be}$, will contribute at a branching ratio of 45.8% for a $s_{1/2}$ proton decay. About 56.5% of ^{11}B states can directly produce one or more neutrons from the listed exclusive modes. All exclusive de-excitation modes with a branching ratio of less than 0.5% and non-exclusive de-excitation processes have been classified as the other modes. It is found that the multiplicities of n, p, d, t, h, α emissions are 1.35, 1.02, 0.54, 0.30, 0.18 and 0.35 for the other modes, respectively. The other modes mainly originate from the ^{11}B states with $E_x > 50$ MeV since the excitation energy is enough to break the ^{11}B nucleus into pieces. In Fig. 4, we plot the kinetic energy distributions of six kinds of outgoing particles from both the exclusive modes and the other modes. Then one can obtain the average kinetic energies 6.6, 7.7, 7.0, 8.0, 8.5 and 6.1 MeV for n, p, d, t, h and α particles, respectively. Based on the neutron kinetic energy distribution in Fig. 4, most of them will give a 2.2 MeV γ -ray from the neutron capture reaction in LS detectors. In addition, the de-excitation modes of $d+^9\text{Be}$ and $d+\alpha+^5\text{He}$ can indirectly produce a neutron from the neutron emission of five discrete levels of ^9Be and the ^5He decay.

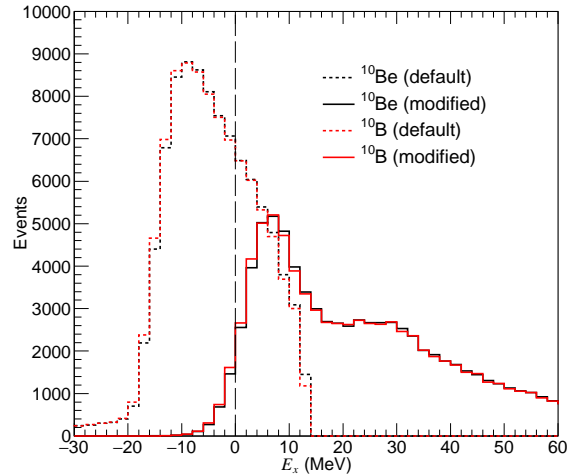


FIG. 5. Excitation energy spectra of ^{10}B and ^{10}Be in the default and modified GENIE.

B. De-excitation processes of ^{10}B and ^{10}Be states

In the above subsection, we only consider the de-excitation processes of the residual nucleus ^{11}B . Other residual nuclei can also be produced through the FSI. Due to the strong interaction, the daughter mesons from the proton decay may interact with spectator nucleons before escaping from the residual nucleus surface. In this case, the FSI can knock the struck nucleon out of ^{11}B , and the residual nucleus is converted to the ^{10}B or ^{10}Be nucleus. The multiple FSI can result in other residual nuclei, such as ^9B , ^9Be , and ^8Li , etc. Here we focus on the de-excitation processes of ^{10}B and ^{10}Be states.

In the default GENIE, the spectator nucleon is on-shell and its energy is given by

$$E_N = \sqrt{m_N^2 + k_2^2}, \quad (4)$$

where m_N is the nucleon mass and the momentum k_2 is same with the red line in the top panel of Fig. 1. With the help of Eqs. (1) and (4), one can calculate the invariant masses of ^{10}B and ^{10}Be through

$$M_{inv} = \sqrt{(M_{12\text{C}} - E_p - E_N + E_b)^2 - (\vec{k}_1 + \vec{k}_2)^2}. \quad (5)$$

Since Eq.(4) overestimates the energy of spectator nucleon, the default GENIE uses a fixed binding energy $E_b = 25$ MeV to offset the reduction of residual nucleus energy. Then the excitation energy spectra of ^{10}B and ^{10}Be states can be easily obtained from $E_x = M_{inv} - M_R$ as shown in Fig. 5, where M_R is the corresponding mass in the ground state. It is clear that the average excitation energy $\langle E_x \rangle$ is negative in the default GENIE case.

In order to solve the $\langle E_x \rangle < 0$ problem, we modify the spectator nucleon energy with

$$E_N = m_N - \bar{E}_R, \quad (6)$$

TABLE IV. De-excitation modes, corresponding thresholds and branching ratios from the de-excitation of ^{10}B states.

De-excitation Mode	Threshold (MeV)	Branching ratio (%)
$\gamma + ^{10}\text{B}$	0	12.2
$n + ^9\text{B}$	8.4	4.9
$p + ^9\text{Be}$	6.6	7.1
$d + ^8\text{Be}$	6.0	8.0
$t + ^7\text{Be}$	18.7	0.6
$h + ^7\text{Li}$	17.8	0.6
$\alpha + ^6\text{Li}$	4.5	10.3
$2n + ^8\text{B}$	27.0	0.6
$n + p + ^8\text{Be}$	8.3	11.2
$2p + ^8\text{Li}$	23.5	0.8
$n + d + ^7\text{Be}$	24.9	1.6
$p + d + ^7\text{Li}$	23.3	1.7
$p + t + ^6\text{Li}$	24.3	1.1
$n + h + ^6\text{Li}$	25.0	1.1
$n + \alpha + ^5\text{Li}$	10.1	1.9
$p + \alpha + ^5\text{He}$	8.9	2.3
$2n + p + ^7\text{Be}$	27.2	0.6
$n + 2p + ^7\text{Li}$	25.5	1.0
$n + p + d + ^6\text{Li}$	30.5	1.0
$p + d + t + \alpha$	25.7	0.5
$2n + 2p + ^6\text{Li} + \alpha$	26.5	0.5
other modes	-	30.6

TABLE V. The percentage of the ground state and discrete states for every daughter nucleus in Table IV from the de-excitation of ^{10}B states. The definition of ratio R_A can be found in Sec. III A.

Nucleus	g.s	1st	2nd	3rd	4th	5th	R_A
^{10}B	22.4	13.9	10.6	16.6	23.2	13.4	0.097
^9B	33.3	17.9	13.6	12.8	12.9	9.5	0.169
^8B	34.7	33.2	14.6	17.5	-	-	0.078
^9Be	41.3	17.4	11.6	11.2	10.2	8.3	0.198
^8Be	47.0	39.9	4.0	3.2	3.0	2.8	0.827
^7Be	36.5	34.2	10.0	8.3	7.5	3.5	0.215
^8Li	34.8	31.7	14.3	19.2	-	-	0.084
^7Li	46.7	35.0	9.9	8.4	-	-	0.213
^6Li	66.6	16.2	6.6	1.1	-	-	0.844

where the removal energy E_R is given by the SF nuclear model [24]. Due to the absence of the ^{11}B spectral function in GENIE, we assume spectator nucleons in ^{11}B have the same SF distribution with protons in ^{12}C . In this case, the invariant masses of the residual nuclei ^{10}B and ^{10}Be can be derived from

$$M_{inv} = \sqrt{(M_{^{12}\text{C}} - E_p - E_N)^2 - (\vec{k}_1 + \vec{k}_2)^2}. \quad (7)$$

Using $E_x = M_{inv} - M_R$, we plot the E_x spectra of ^{10}B

TABLE VI. De-excitation modes, corresponding thresholds and branching ratios from the de-excitation of ^{10}Be states.

De-excitation Mode	Threshold (MeV)	Branching ratio (%)
$\gamma + ^{10}\text{Be}$	0	16.3
$n + ^9\text{Be}$	6.8	19.6
$d + ^8\text{Li}$	21.5	0.7
$t + ^7\text{Li}$	17.2	1.2
$\alpha + ^6\text{He}$	7.4	1.2
$2n + ^8\text{Be}$	8.5	10.3
$n + p + ^8\text{Li}$	23.7	1.7
$n + d + ^7\text{Li}$	23.5	3.4
$n + t + ^6\text{Li}$	24.5	1.8
$n + \alpha + ^5\text{He}$	9.1	4.4
$2n + p + ^7\text{Li}$	25.7	1.9
$2n + d + ^6\text{Li}$	32.2	0.8
$n + p + t + ^5\text{He}$	28.9	0.6
$n + d + t + \alpha$	26.0	0.8
other modes	-	35.4

TABLE VII. The percentage of the ground state and discrete states for every daughter nucleus in Table VI from the de-excitation of ^{10}Be states. The definition of ratio R_A can be found in Sec. III A.

Nucleus	g.s	1st	2nd	3rd	4th	5th	R_A
^{10}Be	31.7	41.3	20.0	2.9	2.4	1.7	0.140
^9Be	48.0	16.0	10.8	10.1	8.5	6.6	0.306
^8Be	38.7	47.5	3.8	3.5	3.3	3.2	0.848
^8Li	36.1	31.0	15.2	17.7	-	-	0.095
^7Li	48.0	35.9	8.7	7.4	-	-	0.239
^6Li	47.4	21.4	13.0	18.2	-	-	0.600

and ^{10}Be states in Fig. 5. The difference between the two curves is very small.

About 2.7% ^{10}B or ^{10}Be states will be assumed to be the ground state because of $E_x < 0$. Then we use the TALYS code to estimate the de-excitation processes of ^{10}B and ^{10}Be states based on the $E_x > 0$ distributions. The initial population is equally distributed over both parities and the inputting spin is assumed to zero. The branching ratio of each exclusive de-excitation mode from the residual nuclei ^{10}B and ^{10}Be have been listed in Table IV and Table VI, respectively. The corresponding percentage of the ground state and discrete states for every daughter nucleus can be found in Tables V and VII. About 24.4% ^{10}B and 45.3% ^{10}Be states can directly produce one or more neutrons from the listed exclusive de-excitation modes. For the other modes of ^{10}B (^{10}Be) states, the multiplicities of n, p, d, t, h, α emissions are 1.00, 1.03, 0.42, 0.24, 0.21 and 0.30 (1.15, 0.62, 0.39, 0.29, 0.10 and 0.40), respectively.

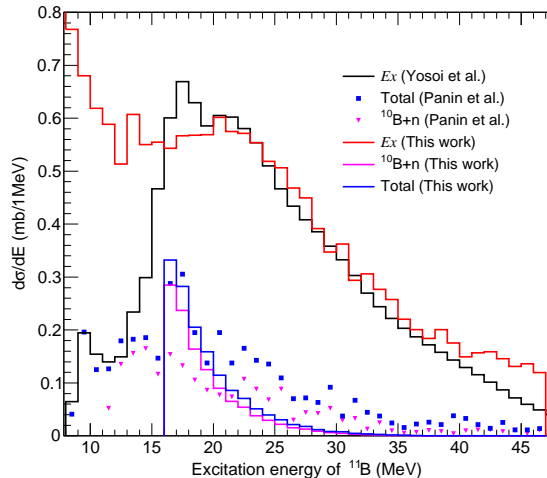


FIG. 6. Comparison of the measured (black line) [30] and predicted (red line) excitation energy spectra of the residual nucleus ^{11}B . The pink triangle (pink line) and blue square (blue line) denote the measured (predicted) results [31] for $^{11}\text{B} \rightarrow n + ^{10}\text{B}$ and all three two-body de-excitation modes, respectively.

IV. COMPARISON WITH EXPERIMENTAL DATA

In order to study the properties of proton-hole states in ^{11}B , the quasifree $^{12}\text{C}(p, 2p)^{11}\text{B}$ [30, 31] and $^{12}\text{C}(e, e'p)^{11}\text{B}$ [23] reactions have been extensively investigated. Yosoi et al. measured the excitation energy spectrum of the proton-hole states in ^{11}B through the quasifree $^{12}\text{C}(p, 2p)^{11}\text{B}$ reaction [30]. As shown in Fig. 6, the predicted E_x curve (red line) from Fig. 3 can well describe the measured one (black line) in the region of $15 \text{ MeV} \leq E_x \leq 40 \text{ MeV}$. Note that the measured E_x spectrum from Ref. [30] has been binned and scaled by an arbitrary factor to match the peak around 10 MeV in Fig. 4 of Ref. [31]. For the convenience of following discussions, we have also scaled the predicted E_x spectrum to match the scaled Yosoi spectrum. For $E_x < 15 \text{ MeV}$, the predicted spectrum is inconsistent with the experimental measurement, and displays a continuous distribution as shown in Fig. 3. It can not explain several discrete peaks in Fig. 1a of Ref. [30]. This is because that we use the continuous spectral function to calculate the excitation energy.

In Ref. [31], Panin et al. measured three de-excitation modes of ^{11}B states from the $^{12}\text{C}(p, 2p)^{11}\text{B}$ reaction, namely $^{11}\text{B} \rightarrow n + ^{10}\text{B}$, $^{11}\text{B} \rightarrow d + ^9\text{Be}$ and $^{11}\text{B} \rightarrow \alpha + ^7\text{Li}$. The $^{11}\text{B} \rightarrow n + ^{10}\text{B}$ (pink triangle) and total (blue square) spectra have been plotted in Fig. 6. For comparison, we use the TALYS code to calculate branching ratios of the three de-excitation modes for every excitation energy bin in the range of 16-47 MeV. Besides the ground state, the predicted branching ratios includes the contributions

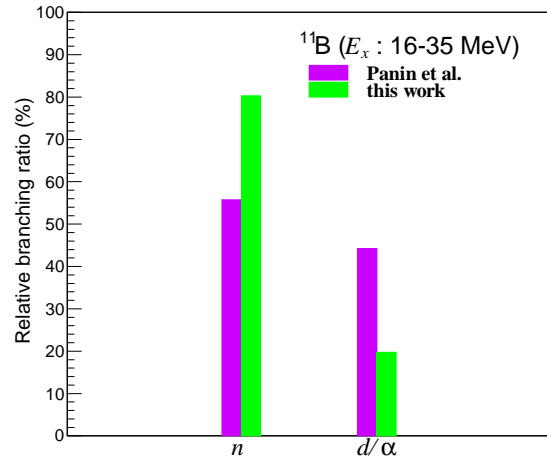


FIG. 7. Comparison of the measured (pink) and predicted (green) relative branching ratios of the n and d/α emissions among all three two-body de-excitation modes from the residual nucleus ^{11}B with $16 \text{ MeV} \leq E_x \leq 35 \text{ MeV}$.

from the first four discrete levels of ^{10}B states, and the first excited level of ^7Li states. In terms of the predicted E_x distribution, we can derive the $^{11}\text{B} \rightarrow n + ^{10}\text{B}$ (pink line) and total (blue line) spectra as shown in Fig. 6. It is clear that the predicted shapes of both the $n + ^{10}\text{B}$ and total spectrum can not describe the measured shapes well. The experimental data of three two-body de-excitation modes in Fig. 6 can be converted into two relative branching ratios of the n and d/α emissions among all three two-body de-excitation modes. The relative branching ratio of n emission can be calculated by dividing the integral of the pink data points in Fig. 6 by the integral of the blue data points. Using the difference between the integrals of the blue and pink data points, one can also derive the relative branching ratio of d/α emission. Note that they are independent of the scale factor. In Fig. 7, we compare the predicted and measured relative branching ratios of the n and d/α emissions for $16 \text{ MeV} \leq E_x \leq 35 \text{ MeV}$. It is found that the predicted n relative branching ratio is larger than the measured one. For the d/α emission, the predicted value can not account for the measured result.

In addition to the excitation energy spectrum, Ref. [30] has also measured the branching ratios of charged particle emissions from the s -hole state in ^{11}B as shown in Fig. 8. The colored areas indicate the branching ratios of decay onto the ‘two-body decay’ regions, and the grey parts mainly come from contributions of three-body and sequential de-excitation modes of ^{11}B states. In Ref. [30], the ‘two-body decay’ regions are defined for each emitted particle species as the excitation energy range in the daughter nucleus between the ground state and the larger of 5 MeV and the threshold for emission of additional particles. The authors have provided simul-

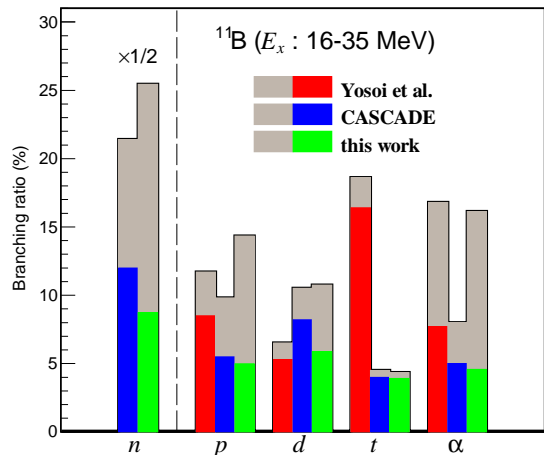


FIG. 8. Comparison of measured and predicted branching ratios of n, p, d, t and α emissions from the residual nucleus ^{11}B with $16 \text{ MeV} \leq E_x \leq 35 \text{ MeV}$. The experimental data (red) were taken from Ref. [30]. The green and blue branching ratios denote the predicted results from the TALYS and CASCADE calculations, respectively.

taneously the results of a statistical model calculation from the CASCADE code [35]. Based on the same definition, we use the TALYS code to calculate the branching ratios of n, p, d, t, α emissions for every E_x bin in the range of 16-35 MeV. Their detection threshold energies are 3.1, 3.1, 4.0, 4.6 and 4.5 MeV, respectively. In addition, the energetic α contribution from the decay of discrete levels of the daughter nucleus ^8Be has been considered. With the help of the E_x distribution between 16-35 MeV, we estimate the branching ratios of n, p, d, t and α emissions from the residual nucleus ^{11}B . In Fig. 8, the green and blue branching ratios denote the TALYS and CASCADE results, respectively. It is found that the predicted branching ratio of each particle emission is basically consistent with the experimental data except for the t emission. The TALYS and CASCADE codes derive

similar results for all ‘two-body decay’ modes. For the key n emission, TALYS give the larger total branching ratio than CASCADE.

V. SUMMARY

In summary, we have investigated the de-excitation processes of the residual nuclei associated with proton decays in ^{12}C based on the GENIE generator and TALYS code. Since the residual nucleus ^{11}B would be left in the ground state, the default GENIE nucleon decay generator has been modified in terms of the SF nuclear model. After deriving the excitation energy spectra of ^{11}B , ^{10}B and ^{10}Be , we use the TALYS code to implement their de-excitation processes. For the s -hole state in ^{11}B , we compare the predicted results with the experimental measurements. It is found that the predicted results are partly consistent with the experimental data. For p, d and α emissions, the predicted branching ratios can basically account for the Yosoi measurement. The TALYS and CASCADE calculations give the similar results for all ‘two-body decay’ modes. For the n emission, the predicted shape from $^{11}\text{B} \rightarrow n + ^{10}\text{B}$ can not describe the measured shape well. For LS experiments, the total n branching ratio from the residual nucleus ^{11}B is the most crucial quantity due to the neutron capture. However, it has not been measured up to now. We hope that future experiments can measure the total branching ratio including one or more neutrons from de-excitation processes of the residual nucleus ^{11}B .

ACKNOWLEDGMENTS

We are grateful to Jie Cheng, Xianguo Lu, Yufeng Li, Yuhang Guo, Benda Xu and Aiqiang Zhang for their helpful discussions. This work is supported in part by the National Nature Science Foundation of China (NSFC) under Grants No. 11575201, No. 11675273 and No. 11775316, and the Strategic Priority Research Program of the Chinese Academy of Sciences under Grant No. XDA10010100.

-
- [1] H. Georgi and S. L. Glashow, Phys. Rev. Lett. **32**, 438-441 (1974) doi:10.1103/PhysRevLett.32.438
 - [2] P. Nath and P. Fileviez Perez, Phys. Rept. **441**, 191-317 (2007) doi:10.1016/j.physrep.2007.02.010 [arXiv:hep-ph/0601023 [hep-ph]].
 - [3] P. A. Zyla *et al.* [Particle Data Group], PTEP **2020**, no.8, 083C01 (2020) doi:10.1093/ptep/ptaa104
 - [4] K. S. Babu, E. Kearns, U. Al-Binni, S. Banerjee, D. V. Baxter, Z. Berezhiani, M. Bergevin, S. Bhattacharya, S. Brice and R. Brock, *et al.* [arXiv:1311.5285 [hep-ph]].
 - [5] K. Abe *et al.* [Hyper-Kamiokande], [arXiv:1805.04163 [physics.ins-det]].
 - [6] F. An *et al.* [JUNO Collaboration], J. Phys. G **43**, no. 3, 030401 (2016) doi:10.1088/0954-3899/43/3/030401 [arXiv:1507.05613 [physics.ins-det]].
 - [7] A. Abusleme *et al.* [JUNO], [arXiv:2104.02565 [hep-ex]].
 - [8] R. Acciarri *et al.* [DUNE], [arXiv:1512.06148 [physics.ins-det]].
 - [9] C. L. Cowan, F. Reines, F. B. Harrison, H. W. Kruse and A. D. McGuire, Science **124**, 103 (1956). doi:10.1126/science.124.3212.103

- [10] K. Eguchi *et al.* [KamLAND Collaboration], Phys. Rev. Lett. **90**, 021802 (2003) doi:10.1103/PhysRevLett.90.021802 [hep-ex/0212021].
- [11] F. P. An *et al.* [DAYA-BAY Collaboration], Phys. Rev. Lett. **108**, 171803 (2012) [arXiv:1203.1669 [hep-ex]].
- [12] M. Wurm *et al.* [LENA Collaboration], Astropart. Phys. **35**, 685 (2012) doi:10.1016/j.astropartphys.2012.02.011 [arXiv:1104.5620 [astro-ph.IM]].
- [13] H. O. Back *et al.* [Borexino], Phys. Lett. B **563**, 23-34 (2003) doi:10.1016/S0370-2693(03)00636-1 [arXiv:hep-ex/0302002 [hep-ex]].
- [14] T. M. Undagoitia, F. von Feilitzsch, M. Goggerneff, C. Grieb, K. A. Hochmuth, L. Oberauer, W. Potzel and M. Wurm, Phys. Rev. D **72**, 075014 (2005) doi:10.1103/PhysRevD.72.075014 [arXiv:hep-ph/0511230 [hep-ph]].
- [15] T. Araki *et al.* [KamLAND], Phys. Rev. Lett. **96**, 101802 (2006) doi:10.1103/PhysRevLett.96.101802 [arXiv:hep-ex/0512059 [hep-ex]].
- [16] K. Asakura *et al.* [KamLAND], Phys. Rev. D **92**, no.5, 052006 (2015) doi:10.1103/PhysRevD.92.052006 [arXiv:1505.03612 [hep-ex]].
- [17] K. Abe *et al.* [Super-Kamiokande], Phys. Rev. D **90**, no.7, 072005 (2014) doi:10.1103/PhysRevD.90.072005 [arXiv:1408.1195 [hep-ex]].
- [18] C. Andreopoulos, A. Bell, D. Bhattacharya, F. Cavanna, J. Dobson, S. Dytman, H. Gallagher, P. Guzowski, R. Hatcher and P. Kehayias, *et al.* Nucl. Instrum. Meth. A **614**, 87-104 (2010) doi:10.1016/j.nima.2009.12.009 [arXiv:0905.2517 [hep-ph]]; C. Andreopoulos, C. Barry, S. Dytman, H. Gallagher, T. Golan, R. Hatcher, G. Perdue and J. Yarba, [arXiv:1510.05494 [hep-ph]].
- [19] L. Alvarez-Ruso *et al.* [GENIE], Eur. Phys. J. ST **230**, no.24, 4449-4467 (2021) doi:10.1140/epjs/s11734-021-00295-7 [arXiv:2106.09381 [hep-ph]].
- [20] A. Bodek and J. L. Ritchie, Phys. Rev. D **24**, 1400 (1981) doi:10.1103/PhysRevD.24.1400
- [21] H. Ejiri, Phys. Rev. C **48**, 1442-1444 (1993) doi:10.1103/PhysRevC.48.1442
- [22] Y. A. Kamyshkov and E. Kolbe, Phys. Rev. D **67**, 076007 (2003) doi:10.1103/PhysRevD.67.076007 [arXiv:nucl-th/0206030 [nucl-th]].
- [23] K. Nakamura, S. Hiramatsu, T. Kamae, H. Muramatsu, N. Izutsu and Y. Watase, Nucl. Phys. A **268**, 381-407 (1976) doi:10.1016/0375-9474(76)90539-X
- [24] O. Benhar, N. Farina, H. Nakamura, M. Sakuda and R. Seki, Phys. Rev. D **72**, 053005 (2005) doi:10.1103/PhysRevD.72.053005 [arXiv:hep-ph/0506116 [hep-ph]].
- [25] A. J. Koning and D. Rochman, Nucl. Data Sheets **113**, 2841-2934 (2012) doi:10.1016/j.nds.2012.11.002
- [26] A. Bodek and T. Cai, Eur. Phys. J. C **79**, no.4, 293 (2019) doi:10.1140/epjc/s10052-019-6750-3 [arXiv:1801.07975 [nucl-th]].
- [27] T. Cai *et al.* [MINERvA], Phys. Rev. D **101**, no.9, 092001 (2020) doi:10.1103/PhysRevD.101.092001 [arXiv:1910.08658 [hep-ex]].
- [28] K. Abe *et al.* [T2K], Phys. Rev. D **98**, no.3, 032003 (2018) doi:10.1103/PhysRevD.98.032003 [arXiv:1802.05078 [hep-ex]].
- [29] X. G. Lu *et al.* [MINERvA], Phys. Rev. Lett. **121**, no.2, 022504 (2018) doi:10.1103/PhysRevLett.121.022504 [arXiv:1805.05486 [hep-ex]].
- [30] M. Yosoi, H. Akimune, I. Daito, H. Ejiri, H. Fujimura, M. Fujiwara, T. Ishikawa, M. Itoh, T. Kawabata and M. Nakamura, *et al.* Phys. Lett. B **551**, 255-261 (2003) doi:10.1016/S0370-2693(02)03062-9
- [31] V. Panin, J. T. Taylor, S. Paschalis, F. Wamers, Y. Aksyutina, H. Alvarez-Pol, T. Aumann, C. A. Bertulani, K. Boretzky and C. Caesar, *et al.* Phys. Lett. B **753**, 204-210 (2016) doi:10.1016/j.physletb.2015.11.082
- [32] J. Cheng, Y. F. Li, L. J. Wen and S. Zhou, Phys. Rev. D **103**, no.5, 053001 (2021) doi:10.1103/PhysRevD.103.053001 [arXiv:2008.04633 [hep-ph]].
- [33] J. Cheng, Y. F. Li, H. Q. Lu and L. J. Wen, Phys. Rev. D **103**, no.5, 053002 (2021) doi:10.1103/PhysRevD.103.053002 [arXiv:2009.04085 [hep-ex]].
- [34] NNDC, "Nuclear structure and decay data", <https://www.nndc.bnl.gov/nudat3/>.
- [35] F. Pühlhofer, Nucl. Phys. A **280**, 267-284 (1977) doi:10.1016/0375-9474(77)90308-6; M. N. Harakeh, *Extended Version of Code CASCADE*, (1983) (unpublished)